

# A Conductance-Based Neuronal Network Model for Color Coding in the Primate Foveal Retina

Pablo Martínez-Cañada<sup>1,2</sup>(✉), Christian Morillas<sup>1,2</sup>, and Francisco Pelayo<sup>1,2</sup>

<sup>1</sup> Department of Computer Architecture and Technology,  
University of Granada, Granada, Spain  
{pablomc, cmg, fpelayo}@ugr.es

<sup>2</sup> Centro de Investigación en Tecnologías de la Información y de las  
Comunicaciones (CITIC), University of Granada, Granada, Spain

**Abstract.** Descriptive models of the retina have been essential to understand how retinal neurons convert visual stimuli into a neural response. With recent advancements of neuroimaging techniques, availability of an increasing amount of physiological data and current computational capabilities, we now have powerful resources for developing biologically more realistic models of the brain. In this work, we implemented a two-dimensional network model of the primate retina that uses conductance-based neurons. The model aims to provide neuroscientists who work in visual areas beyond the retina with a realistic retinal model whose parameters have been carefully tuned based on data from the primate fovea and whose response at every stage of the model adequately reproduces neuronal behavior. We exhaustively benchmarked the model against well-established visual stimuli, showing spatial and temporal responses of the model neurons to light flashes, which can be disk- or ring-shaped, and to sine-wave gratings of varying spatial frequency. The model describes the red-green and blue-yellow color opponency of retinal cells that connect to parvocellular and koniocellular cells in the Lateral Geniculate Nucleus (LGN), respectively. The model was implemented in the widely used neural simulation tool NEST and the code has been released as open source software.

**Keywords:** Primate retina model · Conductance-based neuronal network · Parvocellular pathway · Koniocellular pathway · Red-green color opponency · Blue-yellow color opponency · NEST simulation

## 1 Introduction

The majority of retina models basically fall into two categories. The first one consists of descriptive or phenomenological models [3, 8, 31], which are filter functions that convert input visual stimuli into some neuronal response, commonly recorded from ganglion cells. While they involve just a few parameters whose values are easily calculated from experiments, these models retain only some gross features of the retina and it is hard to construct a qualitative interpretation of

the retinal network behavior. The second category, known as mechanistic models [11, 27], attempts to incorporate known morphological and physiological data of the system. The challenge to construct them lies in finding precise values of all their parameters, provided also that some of them cannot be reliably acquired. Model neurons are formulated in terms of differential equations, whose numerical resolution entails a considerable increase of the computational load. There are also hybrid models that combine descriptive filters in some stages of their circuit, where the response can be approximated by a linear function, with more detailed neuron models in those other stages that exhibit nonlinear responses [20, 21, 34].

While descriptive models have proven to be successful in explaining the general properties of the visual system, improvement of computational technologies and neuroimaging techniques allows implementation of large-scale biophysical models that can facilitate the understanding of its structural and dynamic complexity [13, 14]. However, there are two key limiting factors that continue to hinder the development of biophysical models of the primate retina. One of them is the scarcity of physiological data from primates. The second factor is the lack of standardized neuron models for neurons that communicate via graded potentials instead of spikes, as happens with retinal neurons. Moreover, existing biophysical models of the primate retina [12, 23] are not exhaustively benchmarked against well-established visual stimuli.

To address these challenges, we implemented a two-dimensional network model of the primate retina built on conductance-based neurons. We show spatial and temporal responses of the model neurons to well-known visual stimuli, e.g., light flashes and sine-wave gratings of varying spatial frequency. Simulated response at every stage of the model was correlated with published physiological data. The circuit model was implemented in NEST v2.11 [26] and the code has been released as open source software [9].

## 2 Methods

### 2.1 Overview of the Network Model

The model is organized in two-dimensional grids of retinal cells synaptically connected as shown in the schematic of Fig. 1A. Each layer is scaled to span a patch of  $2 \text{ deg} \times 2 \text{ deg}$  in the foveal visual field of the primate retina and contains  $40 \times 40$  neurons. The network is driven by the three different types of cones, S, M and L types, which correspond to short-, medium- and long-wavelength light respectively. Response of cones was implemented according to van Hateren's model of primate cones [10] with linear cone-horizontal cell feedback (Fig. 1B). We chose the same generic parameter values given in Table 1 of the reference [10], with the exception of parameter  $g_s$ , which was 0.5 instead of 8.81 to slightly increase the overshoot of the response with a stimulus onset.

All remaining retinal cells (horizontal cells, bipolar cells, amacrine cells and ganglion cells) are implemented as single passive compartments [11, 12]. The membrane potential dynamics are given by:

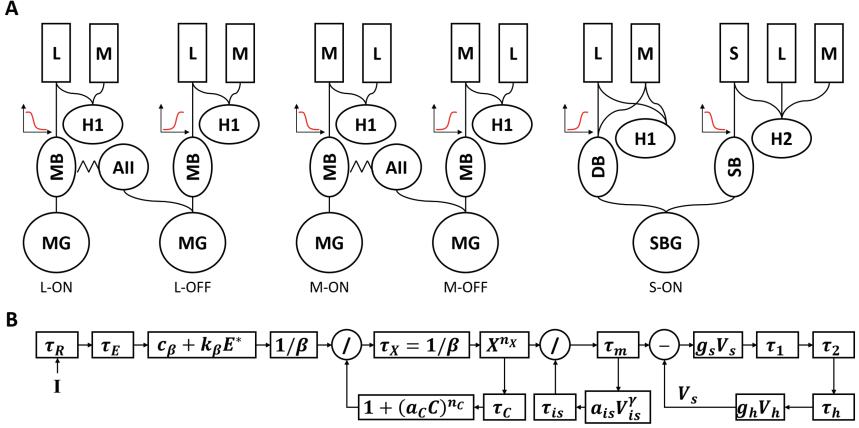


**Fig. 1.** A: Schematic of the circuit model including the different neuron types and connections in the five color opponent pathways: L-ON, L-OFF, M-ON, M-OFF and S-ON. L, M and S are the different types of cones. H1 and H2 are horizontal cells. While H1 type horizontal cells tend to avoid S-cones, H2 cells innervate all types of cones indiscriminately. The different types of bipolar cells are: midget bipolar cell (MB), diffuse bipolar cell (DB) and S-ON bipolar cell (SB). The two types of ganglion cells are: midget ganglion cell (MG) and small bistratified ganglion cell (SBG). ON bipolar cells excite AII macrine cells through gap junctions and, in turn, AII amacrine cells inhibit both OFF bipolar cells and OFF ganglion cells. The different activation functions of the synapse cone-bipolar cell are shown in the insets. B: Model of response of the cone cells consisting of a nonlinearity cascaded with two divisive feedback loops and a subtractive feedback loop [10]. The output of this model, the membrane potential of cones,  $V_s$ , is connected with horizontal cells and bipolar cells.

$$\frac{dV_m(t)}{dt} = -g_L \frac{V_m(t) - E_L}{C_m} - \frac{I_{in}(t)}{C_m} + \frac{I_e}{C_m} \quad (1)$$

where  $V_m(t)$  is the membrane potential of the neuron,  $g_L$  the leak conductance,  $E_L$  the leak reversal potential,  $C_m$  the capacity of the membrane and  $I_e$  a constant external input current. Ganglion cells also include integrate-and-fire dynamics based on a threshold potential,  $V_{th}$ , and a refractory period,  $t_{ref}$ .  $I_{in}(t)$  represents either incoming synaptic currents or gap junction currents. In horizontal cells, bipolar cells and ganglion cells,  $I_{in}(t)$  is the sum of excitatory and inhibitory synaptic currents:

$$I_{in}(t) = \sum_{i=1}^N w_i g_i(t) (V_m(t) - E_{ex}) + \sum_{j=1}^M w_j g_j(t) (V_m(t) - E_{in}) \quad (2)$$

$w_i$ ,  $w_j$  are synaptic weights and  $E_{ex}$ ,  $E_{in}$  are the reversal potentials for the  $N$  excitatory synapses and the  $M$  inhibitory synapses respectively.  $g_i(t)$  and  $g_j(t)$  are the synaptic activation functions of the neuron. Synaptic activation functions are modeled as a direct function of some presynaptic activity measure. In the

simplest case, synaptic interactions are described by an instantaneous sigmoid function [7, 28, 33]:

$$g_i(t) = \frac{1}{1 + e^{-(V_{pre_i}(t) - \theta_{syn})/k_{syn}}} \quad (3)$$

where  $V_{pre_i}(t)$  is the membrane potential of the neuron  $i$  and  $\theta_{syn}$  and  $k_{syn}$  are parameters used to customize the sigmoid function.

By contrast, in amacrine cells,  $I_{in}(t)$  is the sum of gap junction currents through electrical synapses with a constant gap junction conductance ( $g_{gap}$ ):

$$I_{in}(t) = \sum_{i=1}^N g_{gap}(V_m(t) - V_{pre_i}(t)) \quad (4)$$

Photoreceptors release only one type of neurotransmitter, glutamate. However, bipolar cells react to this stimulus with two different responses, ON-center and OFF-center responses [24, 29]. While OFF bipolar cells have ionotropic receptors that maintain light-activated hyperpolarizations of photoreceptors, ON bipolar cells have instead metabotropic receptors that produce a sign reversal at the photoreceptor-ON bipolar cell synapse. Ionotropic glutamate receptors are positively coupled to the synaptic cation channel of OFF bipolar cells, which is opened with an increase of glutamate. On the contrary, ON bipolar cells are negatively coupled to the synaptic cation channel and glutamate acts essentially as an inhibitory transmitter, closing the cation channel.

To simulate the activation function of this cation channel based on the cone membrane potential ( $V_{cone}(t)$ ), we used a sigmoid function whose exponent is negative for OFF bipolar cells (standard sigmoid) and positive for ON bipolar cells (inverted sigmoid):

$$g_{OFF}(t) = \frac{1}{1 + e^{-(V_{cone}(t) - \theta_{syn})/k_{syn}}} \quad (5)$$

$$g_{ON}(t) = \frac{1}{1 + e^{(V_{cone}(t) - \theta_{syn})/k_{syn}}} \quad (6)$$

In the synapse horizontal cell-bipolar cell, although both bipolar cell types express the same ionotropic GABA receptors, GABA release from horizontal cells can evoke opposite responses. One evidence suggests that GABA evokes opposite responses if chloride equilibrium potentials of the synaptic chloride channel in the two bipolar cell types are on opposite sides of the bipolar cell's resting potential [32]. In our model, ON bipolar cells receive excitatory synapses from horizontal cells, which have a positive reversal potential taking as a reference the bipolar cell's resting potential, and OFF bipolar cells receive inhibitory synapses, which have a negative reversal potential.

Among all types of amacrine cells, the model includes only the AII amacrine cell since it is the most studied amacrine cell and the most numerous type in the mammalian retina [18, 22]. The AII amacrine cell is a narrow-field, bistratified

**Table 1.** Parameter values of neuron models.

	$C_m$ (pF)	$g_L$ (nS)	$E_L$ (mV)	$E_{ex}$ (mV)	$E_{in}$ (mV)	$\theta_{syn}$ (mV)	$k_{syn}$	$g_{gap}$ (nS)
Horizontal cell	100	10	-60	0	-	-50	3	-
ON bipolar cell	100	10	-54	0	-70	-35	3	-
OFF bipolar cell	100	10	-45	0	-70	-35	3	-
AII amacrine cell	100	10	-60	-	-	-55	3	10
Ganglion cell	100	10	-62	0	-70	-	-	-

cell that is connected through gap junctions with ON bipolar cells and synaptically innervate OFF cone bipolar terminals and OFF ganglion cell dendrites. The AII amacrine cell plays an essential role in the circuit for rod-mediated (scotopic) vision. However, it is shown that the AII amacrine functionality also extends to cone-mediated (photopic) vision [6, 19]. Under cone-driven conditions, ON cone bipolar cells excite AII amacrine cells through gap junctions and, in turn, AII amacrine cells release inhibitory neurotransmitters onto OFF bipolar cells and OFF ganglion cells. Thus, the AII amacrine network produces crossover inhibition from the ON pathway.

Parameter values of neuron models were chosen as generic as possible (see, for example, values of  $C_m$ ,  $g_L$ ,  $E_{ex}$  and  $E_{in}$  in Table 1). The leak reversal potential,  $E_L$ , was adjusted in horizontal cells and bipolar cells to force a resting potential in the dark of about  $-45$  mV, as observed experimentally [1, 28], and in amacrine cells for a resting potential of about  $-65$  mV. For ganglion cells, we chose values of the leak reversal potential and the threshold potential,  $V_{th}$ , to keep the cell constantly depolarized, resulting in a spontaneous firing rate of about 40 spikes/s. Values of the synaptic activation functions,  $\theta_{syn}$  and  $k_{syn}$ , were set to force a synaptic threshold below resting potential [28].

Synaptic connections were made using the NEST Topology module [25]. In the description of connections shown in Table 2, every cell to the left of the arrow connects to all nodes to the right within a circular mask of radius  $R_s$  and with a delay  $\tau_s$ . Weights of synaptic connections are generated according to a Gaussian distribution of standard deviation  $\sigma_s$ . The sum of the weights of all incoming synapses is equal to the total weight  $W_s$ .

The value of  $\sigma_s$  in the red-green vertical pathway, formed by L and M cones, midget bipolar cells, amacrine cells and midget ganglion cells, corresponds to the radius of the receptive-field center of P cells [4]. The surround of the receptive field is accounted for by horizontal cells. Diffuse bipolar cells contact multiple cones so that their value of  $\sigma_s$  is larger than the receptive field center of P cells but still smaller than the  $\sigma_s$  of horizontal cells. To create the spatially coextensive receptive field of the blue-yellow pathway [5], the value of  $\sigma_s$  of S-ON bipolar cells is the same as that of diffuse bipolar cells. To approximate experimental results [5], both values are set to  $0.05^\circ$ .

Values of synaptic weights were calibrated to reproduce the features of neuronal activity of the primate retina but always keeping  $W_s$  between 1 and 10 nS.

**Table 2.** Parameter values of synaptic connections.

	$R_s$ (deg)	$W_s$ (nS)	$\sigma_s$ (deg)	$\tau_s$ (ms)
L-Cone $\rightarrow$ L-ON MB	0.09	3	0.03	1
L-Cone $\rightarrow$ L-OFF MB	0.09	2.5	0.03	1
L-Cone $\rightarrow$ DB	0.15	1	0.05	1
S-Cone $\rightarrow$ SB	0.15	3	0.05	1
L-Cone $\rightarrow$ H1	0.3	2	0.1	1
L-Cone $\rightarrow$ H2	0.3	1	0.1	1
S-Cone $\rightarrow$ H2	0.3	2	0.1	1
H1 $\rightarrow$ L-ON MB	0.3	2	0.1	5
H1 $\rightarrow$ L-OFF MB	0.3	-3	0.1	5
H2 $\rightarrow$ SB	0.3	2	0.1	5
H1 $\rightarrow$ DB	0.3	-2	0.1	5
AII $\rightarrow$ L-OFF MB	0.09	-2	0.03	1
AII $\rightarrow$ L-OFF MG	0.09	-2	0.03	1
L-ON MB $\rightarrow$ L-ON MG	0.09	10	0.03	1
L-OFF MB $\rightarrow$ L-ON MG	0.09	10	0.03	1
DB $\rightarrow$ SBG	0.09	5	0.03	1
SB $\rightarrow$ SBG	0.09	5	0.03	1

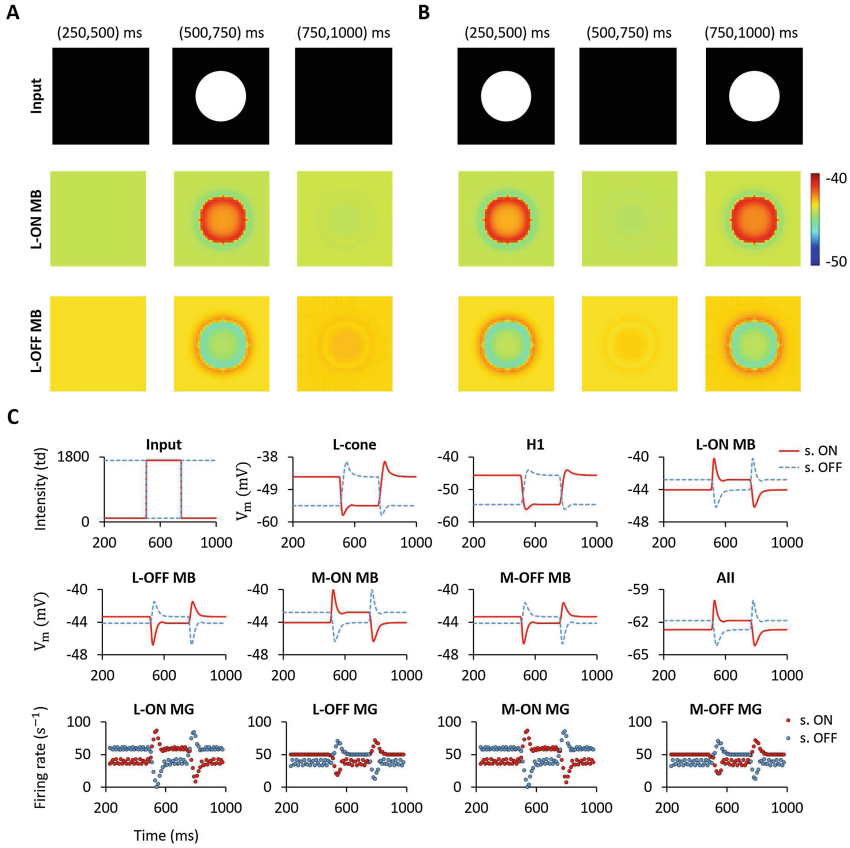
To reproduce the delayed response of the surround, which is measured, on average, between 5 and 15 ms [15], a delay of 5 ms was given to the connection from horizontal cells to bipolar cells.

## 3 Results

### 3.1 Red-Green Pathway

In Fig. 2, we show model responses to a flashing spot of radius  $0.5^\circ$  situated in the center of the grid and covering the whole receptive field of the center neuron. By using a white spot (Fig. 2A) we aim to depict some general spatial properties of the network. The effect of the center-surround antagonism in bipolar cells clearly emerged during the time interval the spot was ON, from 500 to 750 ms. ON bipolar cells at the edge of the spot receive less inhibition from the surround and, thus, showed a marked increase of the response compared to center bipolar cells. The response of OFF bipolar cells at the edge of the spot showed a similar behavior but of opposite sign, resulting in a significant drop below the spontaneous firing. Similar responses were seen for a black spot (Fig. 2B) but with the time windows swapped.

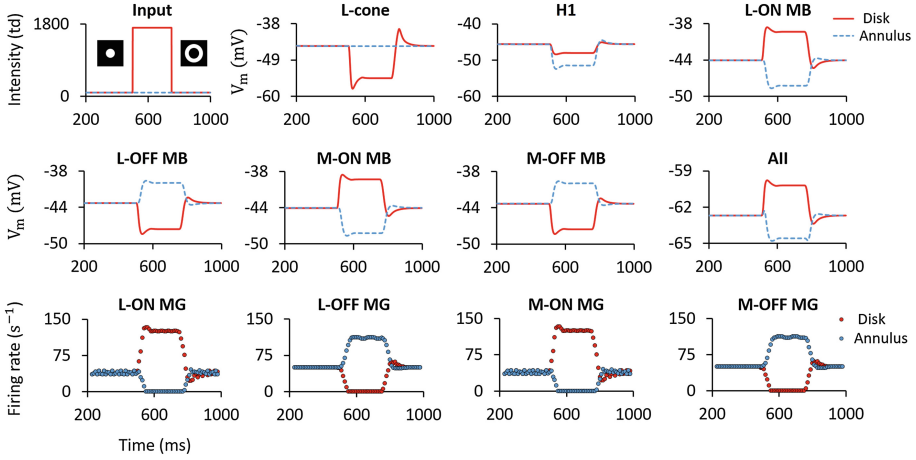
Temporal dynamics of membrane potentials are shown in Fig. 2C. White spots evoked strong depolarizations in ON cells during the stimulus onset, followed by a rebound inhibition for the stimulus offset. Dark stimuli evoked



**Fig. 2.** Time-averaged topographical representation of the membrane potential of L-ON and L-OFF midget bipolar cells to white flashing spots of radius  $0.5^\circ$  (A and B). The intensity of the spots is 1600 trolands (td) and they are superimposed on a spatially uniform background of 100 td. The three time windows at the top are used for averaging the membrane potentials. C: Responses of cells situated in the center of the different neuron grids to the stimulus shown in A (s. ON) and to the stimulus shown in B (s. OFF).

responses of the opposite sign, i.e., pronounced hyperpolarization followed by rebound excitation. This response pattern corresponds to the well-known mechanism of push-pull, inherent to all neurons in the first stages of the visual system. After the overshoot of the response with the stimulus onset, inhibition is able to partially counterbalance the initial excitation within the receptive field and the membrane potential returned close to the resting potential (or spontaneous rate for ganglion cells). The same analysis applies for OFF cells but taking into account that the responses are now of opposite sign.

In the following experiment, we used spots and annuli in order to favor either the center or the surround mechanisms of the receptive field [2] (see



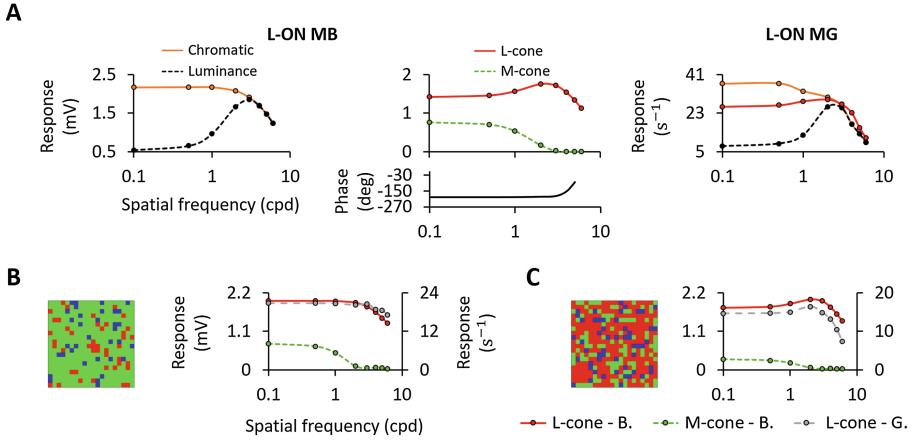
**Fig. 3.** Responses of cells situated in the center of the different neuron grids to a white disk of radius  $0.09^\circ$  and a white annulus with inner and outer radii of  $0.09$  and  $0.5^\circ$  respectively. Stimuli are flashed from 500 to 750 ms.

Fig. 3). Notice that, as a consequence of isolating one of the two mechanisms, the response did not return to the resting potential after the initial overshoot. The center response, activated by the disk stimulus, showed a peak 35 ms after the stimulus onset. The peak of the surround response, activated by the annulus stimulus, was delayed by approximately 10–15 ms with respect to the center response [2].

We simulated spatial frequency responses for luminance, chromatic and cone-isolating gratings (Fig. 4) and our results are correlated with physiological measures [17]. Firstly, for Fig. 4A, the mosaic of cones that describes the spatial distribution of the different cone types in the fovea is spatially uniform, such as the one used so far. One important aspect shown here is how chromatic and luminance signals were multiplexed in low and high spatial frequencies respectively by midget cells in the retina. Thus, the spatial frequency tuning curve with a chromatic grating was low-pass and with a luminance grating was band-pass. The response to the luminance grating showed also a peak at about 3 cpd, as shown for the cell in Fig. 4B of reference [17]. The spatial frequency tuning curves for L- and M-cone-isolating gratings showed different high-frequency cutoffs, a feature consistent with the spatial structure of the receptive field. The response modulation to M- and L-cone-isolating gratings was  $180^\circ$  out of phase as long as the response to the M-cone-isolating grating was nonzero.

However, the response to the L-cone-isolating grating was slightly band-pass, as a consequence of the mixed input of L and M cones we chose for the H1 horizontal cell, prioritizing morphological studies of the primate retina. The majority of cells measured in [17] showed marked low-pass responses though. We thus next asked the question of whether the spatial distribution of the mosaic of cones could influence the response to the L-cone-isolating grating. In Fig. 4B and C, a more





**Fig. 4.** A: Spatial frequency curves of center cells for luminance, chromatic gratings and gratings isolating a receptive field cone class (L-cone and M-cone). Sine-wave gratings are drifted at 2Hz, with a mean luminance level of 1000 td and a contrast of 0.8. The response amplitude corresponds to the first harmonic computed based on Fourier analysis of either the membrane potential or the firing rate. The mosaic of the different cone types is spatially uniform. B: Spatial frequency curves of a cell situated in the center of a retina region with a high density of M-cones. Cones are randomly placed according to an uniform distribution with the following probabilities: 30% of L-cones, 60% of M-cones and 10% of S-cones. C: Spatial frequency curves of a cell situated in a region of the retina with a high density of L-cones. Probabilities are now: 60% of L-cones, 30% of M-cones and 10% of S-cones. L-cone-B. and M-cone-B. are the responses of the midget bipolar cell to the L- and M-cone-isolating gratings. L-cone-G. is the response of the midget ganglion cell to the L-cone-isolating grating.

realistic scenario is presented, in which we randomly situated the different cone types in the grid. We used two different sets of probabilities to simulate either a region of the retina rich in M-cones (Fig. 4B) or a region with a high density of L-cones (Fig. 4C). As expected, the spatial frequency curve for the mosaic in Fig. 4B was low-pass as a result of the considerable degree of cone-specific input to the surround of the receptive field.

### 3.2 Blue-Yellow Pathway

To study the receptive-field structure of retinal cells in the blue-yellow pathway we used cone-isolating stimuli that modulate either S cones or L and M cones independently [5] (Fig. 5). The small bistratified ganglion cell receives S-ON excitatory input from the S-ON bipolar cell and LM-OFF excitatory input from the diffuse bipolar cell. The response pattern of the small bistratified ganglion cell in Fig. 5A correspond to a distinct blue-ON/yellow-OFF opponent cell type.

Receptive fields were further analyzed with drifting sinusoidally modulated gratings that varied in spatial frequency (Fig. 5B). Focusing on the small bistratified ganglion cell, it is shown that both the S and LM spatial frequency

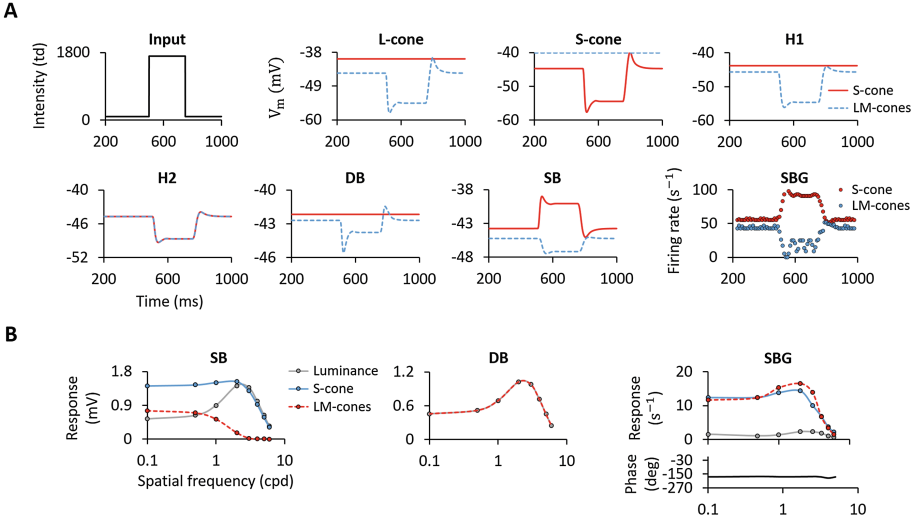


**Fig. 5.** A: Responses of center cells to a  $0.5^\circ$  spot. B: Spatial frequency curves for an uniform cone mosaic.

responses have similar spatial tuning, as a result of the spatially coextensive receptive fields of S-ON and diffuse bipolar cells [5]. These curves were mainly low-pass although a small band-pass resonance peak is observed at 3 cpd that stem from the receptive field surrounds of S-ON and diffuse bipolar cells. Note that the response to the luminance grating is bandpass and it is greatly attenuated. Parameters of the model were chosen to produce similar S and LM spatial frequency responses rather than a more prominent response to the luminance grating as observed in other studies [30].

## 4 Conclusion

We have implemented a conductance-based retina model that incorporates key aspects of the neuroanatomical organization of the primate foveal retina [16]. Most of the parameters correspond to physiological magnitudes that can be measured experimentally. The model aims to provide a coherent account of the response of red-green and blue-yellow color opponent cell types. We have exhaustively benchmarked the model against well-established visual stimuli, showing spatial and temporal responses of the model neurons to light flashes, which can be disk- or ring-shaped, and to sine-wave gratings of varying spatial frequency. By providing a reliable model within which a broad range of neuronal interactions can be examined at several different levels, the model offers a powerful platform for further investigations in visual areas beyond the retina, focusing on color-coding in the primate visual pathway.

**Acknowledgments.** This work was supported by the Spanish National Grant TIN2016-81041-R and the research project P11-TIC-7983 of Junta of Andalucía (Spain), co-financed by the European Regional Development Fund (ERDF). P. Martínez-Cañada was supported by the PhD scholarship FPU13/01487, awarded by the Government of Spain, FPU program.

## References

1. Arman, A.C., Sampath, A.P.: Dark-adapted response threshold of OFF ganglion cells is not set by OFF bipolar cells in the mouse retina. *J. Neurophysiol.* **107**(10), 2649–2659 (2012)
2. Benardete, E.A., Kaplan, E.: The receptive field of the primate P retinal ganglion cell, i: linear dynamics. *Vis. Neurosci.* **14**(01), 169–185 (1997)
3. Berry, M.J., Brivanlou, I.H., Jordan, T.A., Meister, M.: Anticipation of moving stimuli by the retina. *Nature* **398**(6725), 334–338 (1999)
4. Croner, L.J., Kaplan, E.: Receptive fields of P and M ganglion cells across the primate retina. *Vis. Res.* **35**(1), 7–24 (1995)
5. Crook, J.D., Davenport, C.M., Peterson, B.B., Packer, O.S., Detwiler, P.B., Dacey, D.M.: Parallel ON and OFF cone bipolar inputs establish spatially coextensive receptive field structure of blue-yellow ganglion cells in primate retina. *J. Neurosci.* **29**(26), 8372–8387 (2009)
6. Demb, J.B., Singer, J.H.: Intrinsic properties and functional circuitry of the AII amacrine cell. *Vis. Neurosci.* **29**(01), 51–60 (2012)
7. Destexhe, A., Mainen, Z.F., Sejnowski, T.J., et al.: Synaptic currents, neuromodulation, and kinetic models. *Handb. Brain Theory Neural Netw.* **66**, 617–648 (1995)
8. Enroth-Cugell, C., Robson, J.G.: The contrast sensitivity of retinal ganglion cells of the cat. *J. Physiol.* **187**(3), 517–552 (1966)
9. Github: code repository. <https://github.com/pablomc88>
10. van Hateren, H.: A cellular and molecular model of response kinetics and adaptation in primate cones and horizontal cells. *J. Vis.* **5**(4), 5–5 (2005)
11. Hennig, M.H., Funke, K., Wörgötter, F.: The influence of different retinal subcircuits on the nonlinearity of ganglion cell behavior. *J. Neurosci.* **22**(19), 8726–8738 (2002)
12. Hennig, M.H., Wörgötter, F.: Effects of fixational eye movements on retinal ganglion cell responses: a modelling study. *Front. Comput. Neurosci.* **1**, 1–12 (2007)
13. Hill, S., Tononi, G.: Modeling sleep and wakefulness in the thalamocortical system. *J. Neurophysiol.* **93**(3), 1671–1698 (2005)
14. Izhikevich, E.M., Edelman, G.M.: Large-scale model of mammalian thalamocortical systems. *Proc. Nat. Acad. Sci.* **105**(9), 3593–3598 (2008)
15. Kaplan, E., Benardete, E.: The dynamics of primate retinal ganglion cells. *Prog. Brain Res.* **134**, 17–34 (2001)
16. Kolb, H., Fernandez, E., Nelson, R., Jones, B.W.: *Webvision: The Organization of the Retina and Visual System*. National Library of Medicine, Bethesda (2011). Copyright
17. Lee, B.B., Shapley, R.M., Hawken, M.J., Sun, H.: Spatial distributions of cone inputs to cells of the parvocellular pathway investigated with cone-isolating gratings. *JOSA A* **29**(2), A223–A232 (2012)
18. MacNeil, M.A., Masland, R.H.: Extreme diversity among amacrine cells: implications for function. *Neuron* **20**(5), 971–982 (1998)

19. Manookin, M.B., Beaudoin, D.L., Ernst, Z.R., Flagel, L.J., Demb, J.B.: Disinhibition combines with excitation to extend the operating range of the OFF visual pathway in daylight. *J. Neurosci.* **28**(16), 4136–4150 (2008)
20. Martínez-Cañada, P., Morillas, C., Pino, B., Ros, E., Pelayo, F.: A computational framework for realistic retina modeling. *Int. J. Neural Syst.* **26**(07), 1650030 (2016)
21. Martínez-Cañada, P., Morillas, C., Pino, B., Pelayo, F.: Towards a generic simulation tool of retina models. In: Ferrández Vicente, J.M., Álvarez-Sánchez, J.R., de la Paz López, F., Toledo-Moreo, F.J., Adeli, H. (eds.) *IWINAC 2015*. LNCS, vol. 9107, pp. 47–57. Springer, Cham (2015). doi:[10.1007/978-3-319-18914-7\\_6](https://doi.org/10.1007/978-3-319-18914-7_6)
22. Masland, R.H.: The fundamental plan of the retina. *Nat. Neurosci.* **4**(9), 877–886 (2001)
23. Momiji, H., Hankins, M.W., Bharath, A.A., Kennard, C.: A numerical study of red-green colour opponent properties in the primate retina. *Eur. J. Neurosci.* **25**(4), 1155–1165 (2007)
24. Nawy, S., Jahr, C.E.: Suppression by glutamate of cGMP-activated conductance in retinal bipolar cells. *Nature* **346**(6281), 269 (1990)
25. Plesser, H.E., Austvoll, K.: Specification and generation of structured neuronal network models with the NEST topology module. *BMC Neurosci.* **10**(suppl 1), P56 (2009)
26. Plesser, H.E., Diesmann, M., Gewaltig, M.O., Morrison, A.: NEST: the Neural Simulation Tool. In: Jaeger, D., Jung, R. (eds.) *Encyclopedia of Computational Neuroscience*. Springer, Heidelberg (2015). [www.springerreference.com/docs/html/chapterbid/348323.html](http://www.springerreference.com/docs/html/chapterbid/348323.html)
27. Publico, R., Oliveira, R.F., Roque, A.C.: A computational study on the role of gap junctions and rod Ih conductance in the enhancement of the dynamic range of the retina. *PLoS ONE* **4**(9), e6970 (2009)
28. Smith, R.G.: Simulation of an anatomically defined local circuit: the cone-horizontal cell network in cat retina. *Vis. Neurosci.* **12**(03), 545–561 (1995)
29. Snellman, J., Kaur, T., Shen, Y., Nawy, S.: Regulation of ON bipolar cell activity. *Prog. Retinal Eye Res.* **27**(4), 450–463 (2008)
30. Tailby, C., Szmajda, B., Buzas, P., Lee, B., Martin, P.: Transmission of blue (S) cone signals through the primate lateral geniculate nucleus. *J. Physiol.* **586**(24), 5947–5967 (2008)
31. Tranchina, D., Gordon, J., Shapley, R.: Retinal light adaptation-evidence for a feedback mechanism. *Nature* **310**(5975), 314–316 (1984)
32. Vardi, N., Zhang, L.L., Payne, J.A., Sterling, P.: Evidence that different cation chloride cotransporters in retinal neurons allow opposite responses to GABA. *J. Neurosci.* **20**(20), 7657–7663 (2000)
33. Wang, X.J., Rinzal, J.: Alternating and synchronous rhythms in reciprocally inhibitory model neurons. *Neural Comput.* **4**(1), 84–97 (1992)
34. Wohrer, A., Kornprobst, P.: Virtual retina: a biological retina model and simulator, with contrast gain control. *J. Comput. Neurosci.* **26**(2), 219–249 (2009)